Supplementary Information

Piezo-Fenton synergistic effect of ferroelectric single-crystal $BaTiO_3$ nanoparticles for high-efficiency catalytic pollutants degradation in aqueous solution

Hongcheng Gao*[a], Yuanguang Zhang[a], Hongyu Xia[a], Xiaoxia Mao[a], Xiaojing Zhu[b], Shihao Miao[a], Mengqin Shi[a], and Shijiao Zha*[c]

[a]Key Laboratory of Aqueous Environment Protection and Pollution Control of Yangtze River in Anhui of Anhui, Provincial Education Department, College of Resources and Environment, Anqing Normal University, Anqing 246011, China

[b]Research Center of Advanced Chemical Equipment, Chemistry and Chemical Engineering Guangdong Laboratory, Shantou 515041, China

[c]School of Earth and Environment, Anhui University of Science and Technology, Huainan 232001, China

*Corresponding Authors

Email: hongchenggao@aqnu.edu.cn (H. Gao); zhashijiao1991@aust.edu.cn (S. Zha).

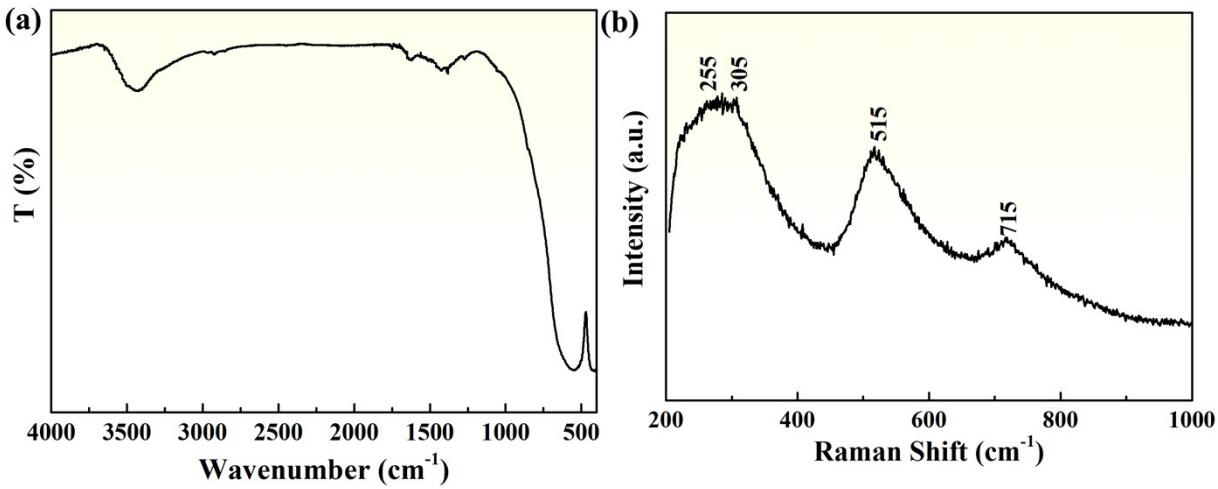

Fig. S1. (a) FT-IR spectra and (b) Raman spectra of BT nanoparticles.

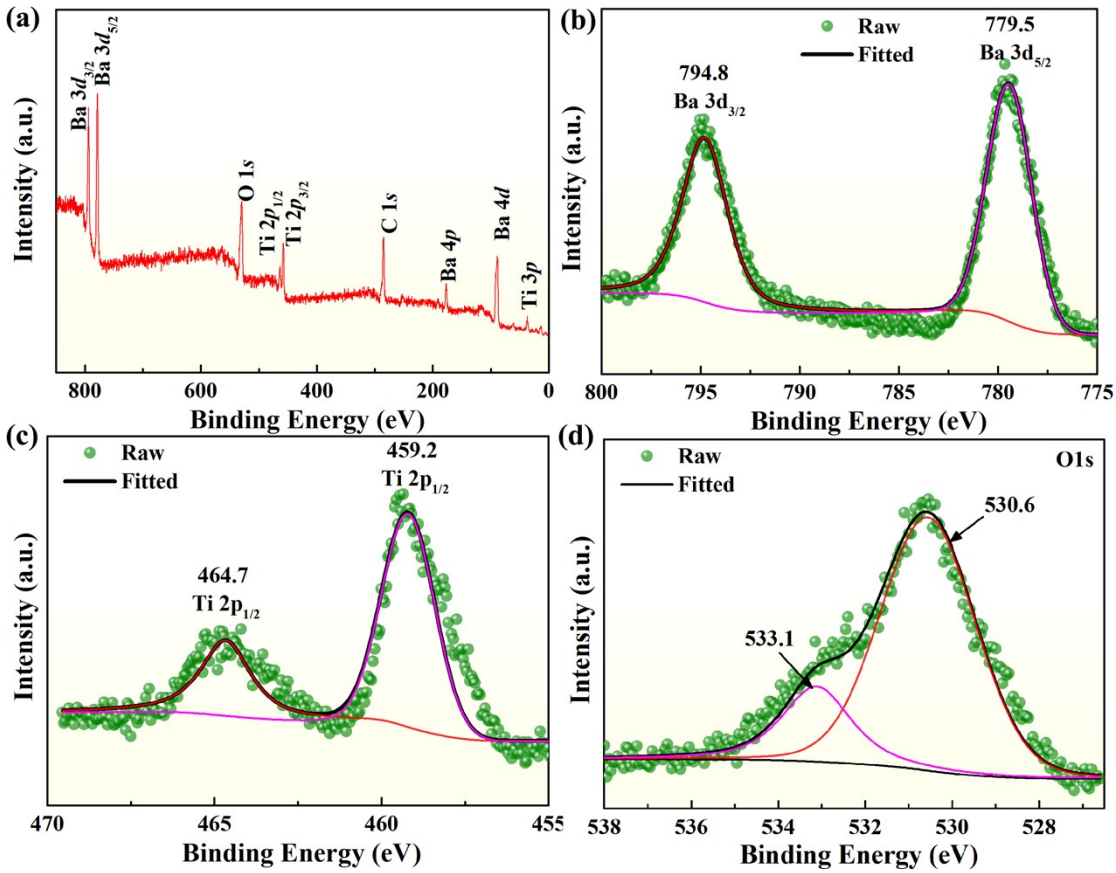

Fig. S2. XPS spectra of BT: (a) survey spectrum, high-resolution spectra of Ba3d (b), Ti 2p (c) and O 1s (d).

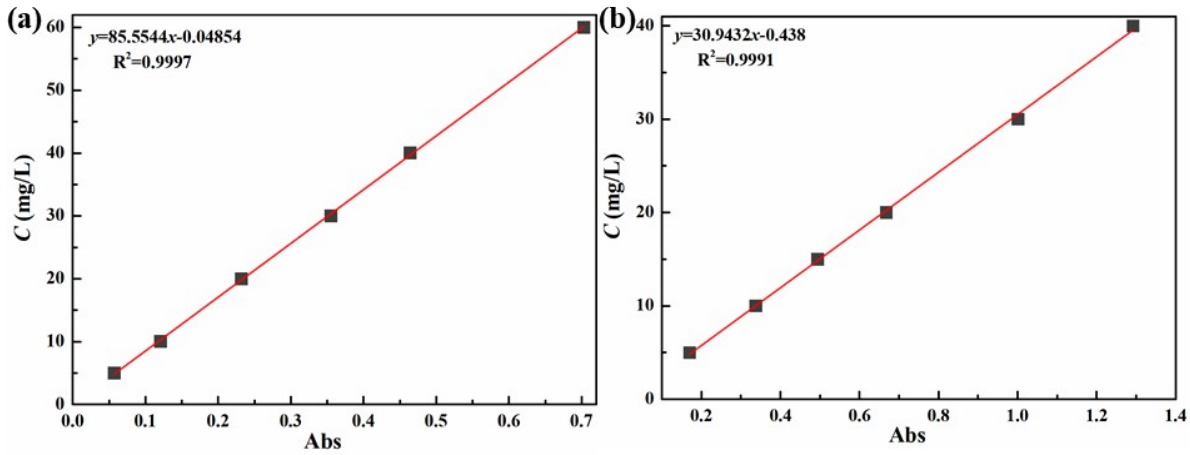

Fig. S3. Standard curves for analyzing different concentrations of (a) CR (5–60 mg/L) and (b)TH (5–40 mg/L) solutions.

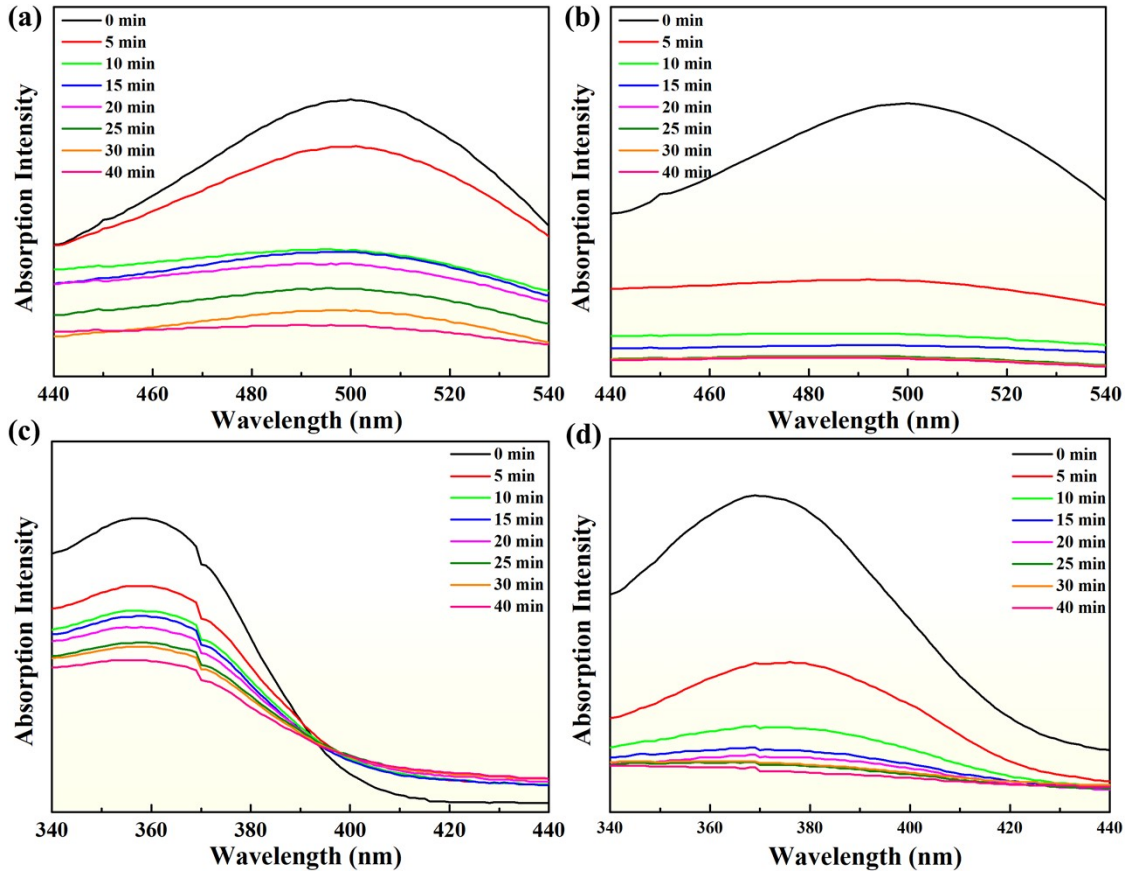

Fig. S4. Aabsorption spectra of the CR solutions (a) C_0 = 30 mg/L and BT = 1 g/L, (b) C_0 = 40 mg/L and BT = 2 g/L. Aabsorption spectra of the TH solutions (c) C_0 = 10 mg/L and BT = 1 g/L, (d) C_0 = 10 mg/L and BT = 3 g/L.

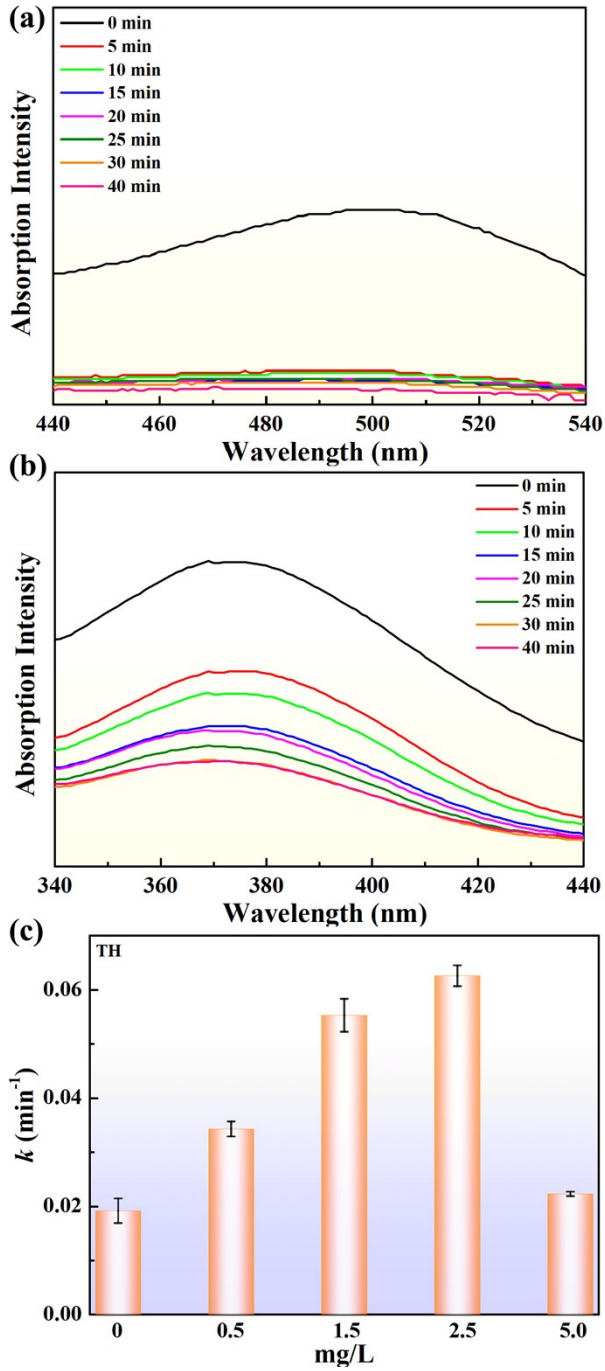

Fig. S5. Absorption spectra of the (a) CR and (b) TH solutions at Fe(II) concentration of 2.5 mg/L. (c) rate constants for TH at different Fe(II) concentrations.

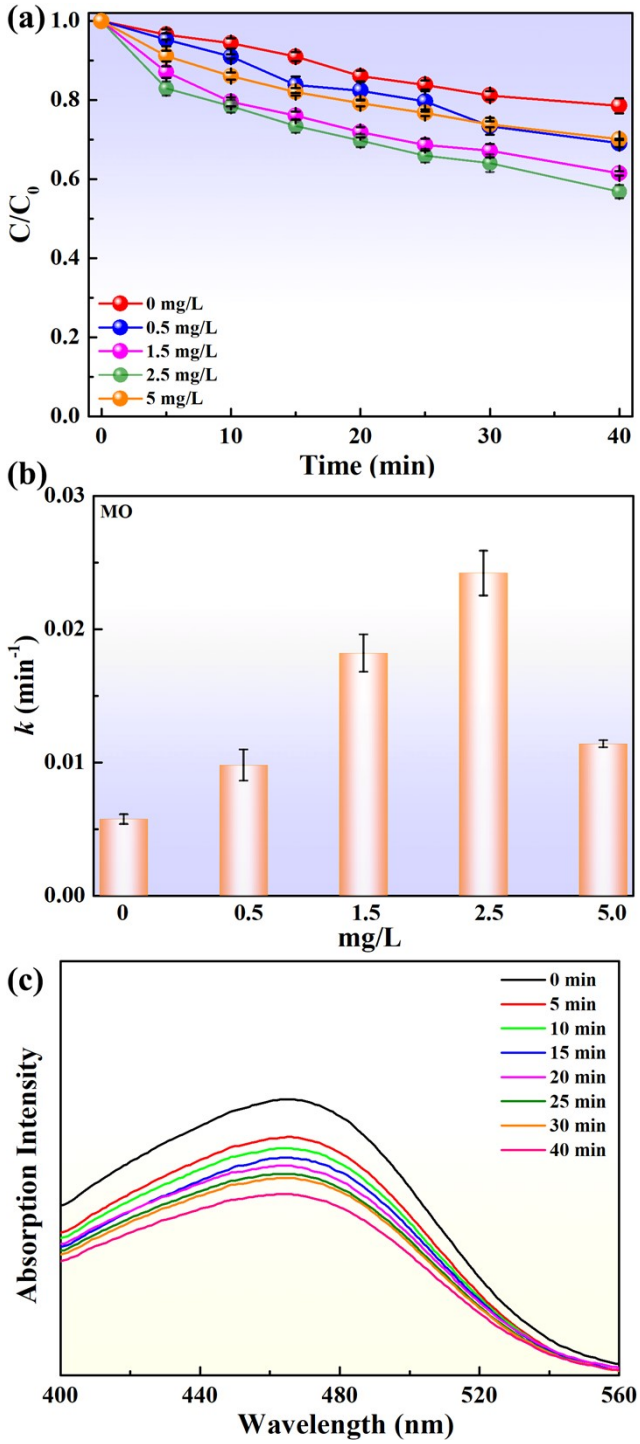

Fig. S6. (a) catalytic degradation curves, and (b) rate constants at different Fe(II) concentrations for MO solutions with initial concentration of 5 mg/L. (c) absorption spectra of the MO solutions at Fe(II) concentration of 2.5 mg/L.

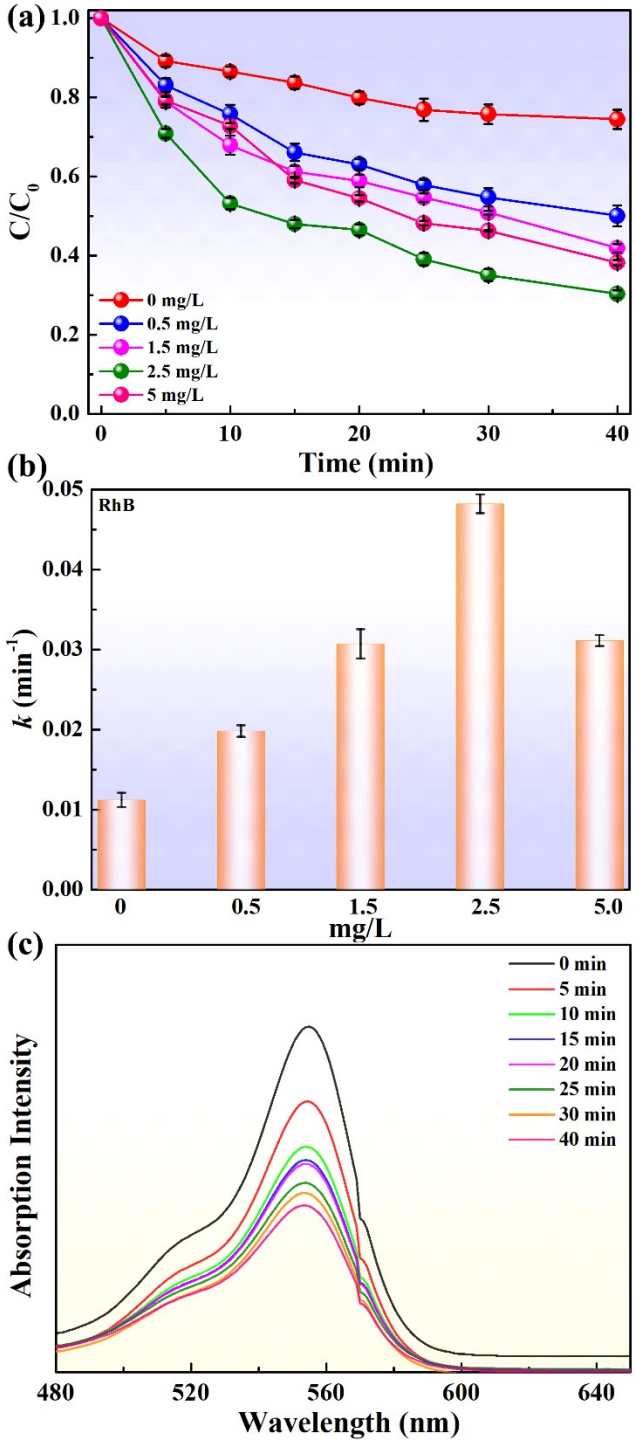

Fig. S7. (a) catalytic degradation curves, and (b) rate constants at different Fe(II) concentrations for RhB solutions with initial concentration of 10 mg/L. (c) absorption spectra of the RhB solutions at Fe(II) concentration of 2.5 mg/L.

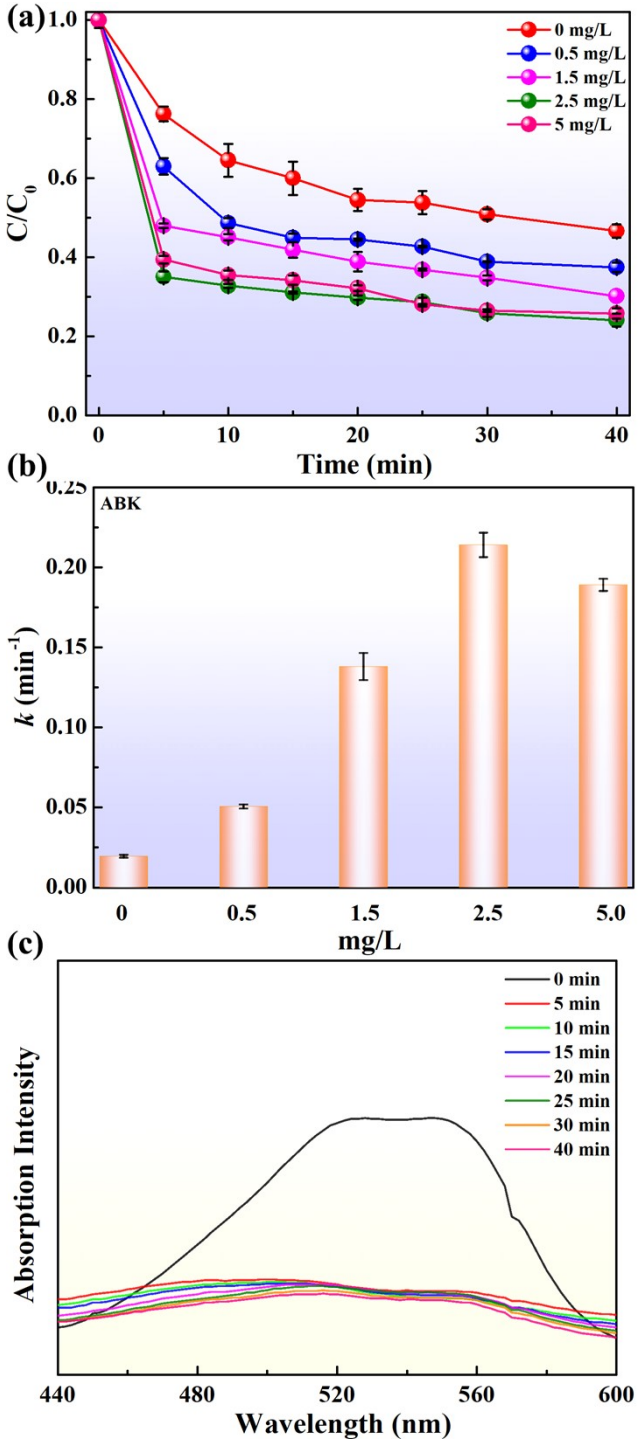

Fig. S8. (a) catalytic degradation curves, and (b) rate constants at different Fe(II) concentrations for ABK solutions with initial concentration of 10 mg/L. (c) absorption spectra of the ABK solutions at Fe(II) concentration of 2.5 mg/L.

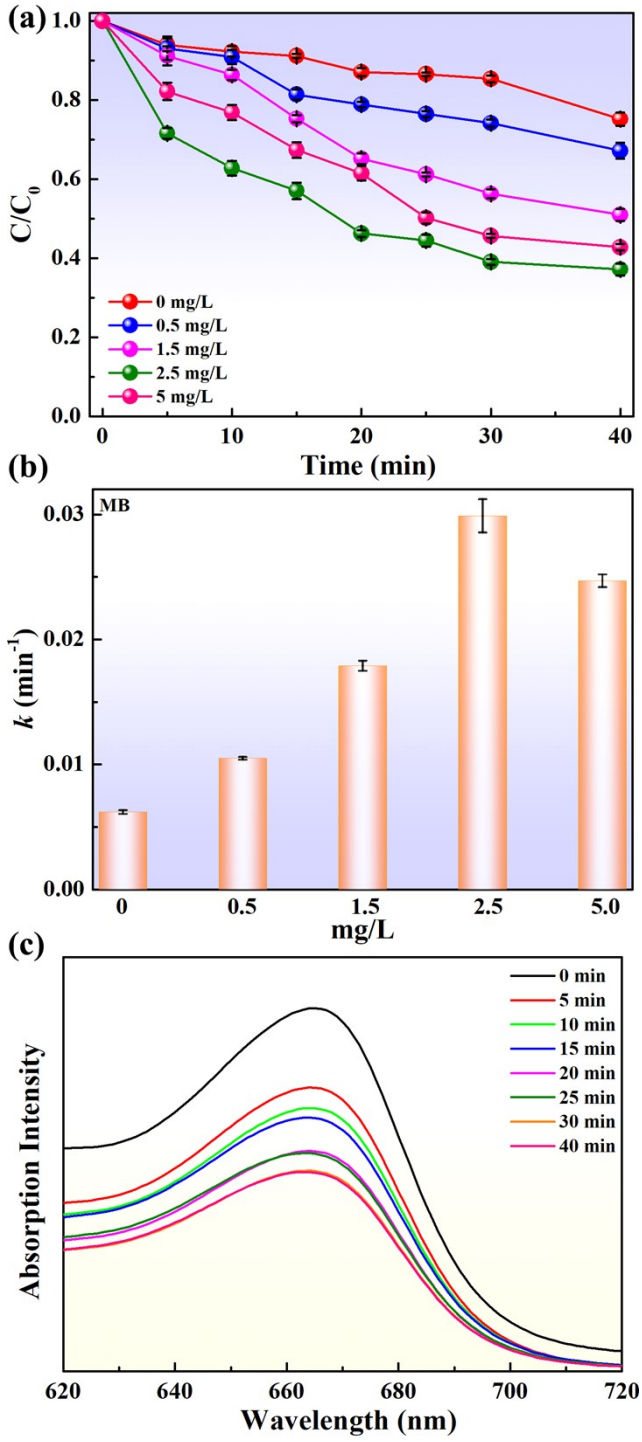

Fig. S9. (a) catalytic degradation curves, and (b) rate constants at different Fe(II) concentrations for MB solutions with initial concentration of 10 mg/L. (c) absorption spectra of the MB solutions at Fe(II) concentration of 2.5 mg/L.

Piezocatalyst	Dye species	Dye concentration (mg/L)	Catalyst dosage (g/L)	Ultrasonic source (kHz/W)	degradation efficiency（%/time (min)	References
$BiFeO_3$ micro-sheets	RhB	10	1	40/*	95/80	[1]
$BaTiO_3$ nanofibers	RhB	5	0.1	40/80	97.5/60	[2]
ZnO/$BaTiO_3$ heterostructures	RhB	10	1	40/120	97/30	[3]
Ag-$BaTiO_3$ heterostructures	RhB	5	1	*	83/75	[4]
$Bi_{0.5}Na_{0.5}TiO_3$ nanorods	RhB	10	1	28/200	95/70	[5]
$Ag_2O/Bi_4Ti_3O_{12}$	RhB	20	1	84/60	71/30	[6]
$(Na_{0.5}Bi_{0.5})TiO_3$-$Ba(Ti_{0.5}Ni_{0.5})O_3$	RhB	10	1	40/200	90/60	[7]
Ag/$BaTiO_3$	RhB	5	1	*/150	93.9/120	[8]
$xBaTiO_3/(1-x)KNbO_3$	DLB5B	*	0.1	45/*	93.3/180	[9]
$BiFeO_3/TiO_2$ p-n heterojunction	TC	10	1	*	72.2/180	[10]
	MB	10	1	*	90.1/180	
$Na_{0.5}Bi_{0.5}TiO_3$ nanoparticles	RhB	10	2	40/150	92/120	[11]
Single-crystal $BaTiO_3$ nanoparticles	CR	10	1	80/50	82.8, 92.2/5,40	This work

Table S1. Comparison of piezocatalytic performance of various piezocatalysts

*unknown

Table S2. The chemical properties of target molecules.

Compound	Formula	Molar mass ($g \cdot mol^{-1}$)	Max rate constant (min^{-1})	degradation efficiency （%）
Methyl orange	$C_{14}H_{14}N_3NaO_3S$	327.33	0.0242	43.1
Methylene blue	$C_{16}H_{18}ClN_3S \cdot 3H_2O$	373.9	0.0299	62.8
Rhodamine B	$C_{28}H_{31}ClN_2O_3$	479.01	0.0482	69.7
Tetracycline hydrochloride	$C_{22}H_{24}N_2O_8 \cdot HCl$	480.9	0.0626	72.6
Acid chrome blue K	$C_{16}H_9N_2Na_3O_{12}S_3$	586.41	0.214	75.9
Congo red	$C_{32}H_{22}N_6Na_2O_6S_2$	696.66	0.337	92.2

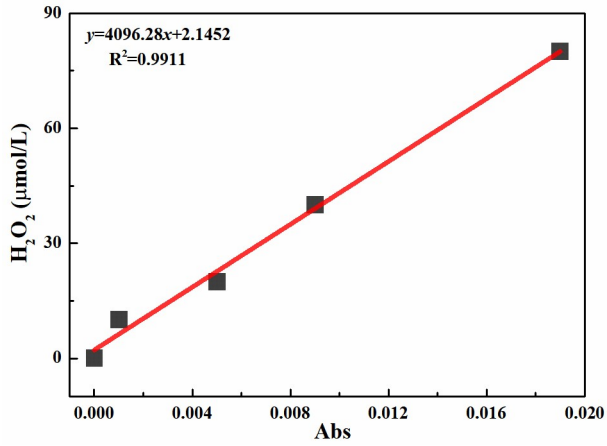

Fig. S10. The standard curves for analyzing different concentrations of H_2O_2 with the Fenton-DPD method.

The Fenton-DPD method is commonly used for the measurement of low H_2O_2 concentrations in aqueous solutions. The steps are as follows [12, 13]:

Standard curve for the determination of H_2O_2: Firstly, 18 mL of pH 3.0 HAC/AC^- buffer stock solution (0.5 M), 5.0 mL of DPD stock solution (100 mM) and 1.5 mL of $FeSO_4$ stock solution (25 mM) were added to a 25 mL beaker flask. Then, 0.5 mL of sample containing different concentrations of H_2O_2 was added under stirring. After 45 s, 3 mL the reaction solution was immediately transferred into 1 cm quartz cells to measure the absorbance at 551 nm. Subsequently, absorbance at 551 nm *vs* H_2O_2 concentration were plotted to obtain the standard curves graph (Fig. S10).

The general procedures to determine the H_2O_2 concentration in BT sample: Firstly, 18 mL of pH 3.0 HAC/AC^- buffer stock solution (0.5 M), 5.0 mL of DPD stock solution (100 mM) and 1.5 mL of $FeSO_4$ stock solution (25 mM) were added to a 25 mL beaker flask. Then, 0.5 mL unknown concentrations of H_2O_2 in sample was mixed with the solution. After 45 s, 3 mL the reaction solution was immediately transferred into 1 cm quartz cells to measure the absorbance at 551 nm. For unknown concentrations of H_2O_2 in sample was determined with from Fig. S10 standard curves.

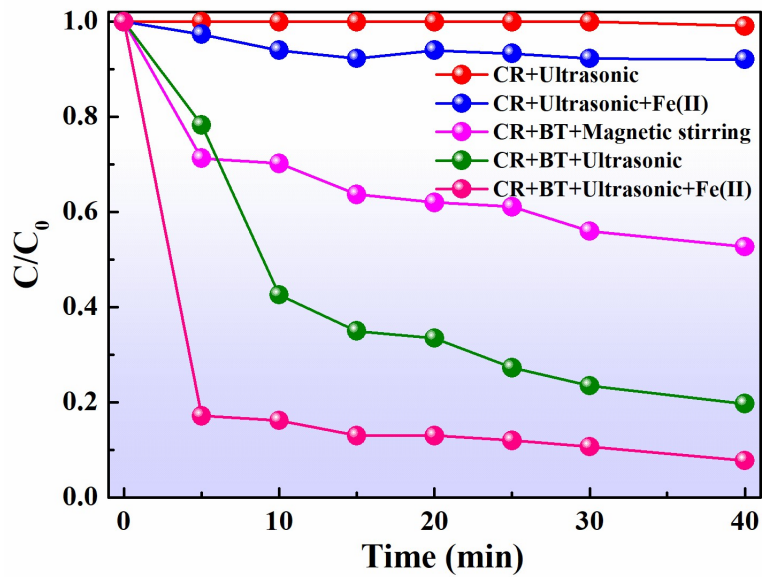

Fig. S11. Degradation curves for CR under different catalytic conditions.

References

[1] H. You, Y. Jia, Z. Wu, X. Xu, W. Qian, Y. Xia, M. Ismail, Strong piezo-electrochemical effect of multiferroic $BiFeO_3$ square micro-sheets for mechanocatalysis, Electrochemistry Communications, 79 (2017) 55-58.

[2] X. Xu, Z. Wu, L. Xiao, Y. Jia, J. Ma, F. Wang, L. Wang, M. Wang, H. Huang, Strong piezo-electro-chemical effect of piezoelectric $BaTiO_3$ nanofibers for vibration-catalysis, Journal of Alloys and Compounds, 762 (2018) 915-921.

[3] X. Zhou, S. Wu, C. Li, F. Yan, H. Bai, B. Shen, H. Zeng, J. Zhai, Piezophototronic effect in enhancing charge carrier separation and transfer in $ZnO/BaTiO_3$ heterostructures for high-efficiency catalytic oxidation, Nano Energy, 66 (2019) 104127.

[4] S. Xu, Z. Liu, M. Zhang, L. Guo, Piezotronics enhanced photocatalytic activities of Ag-$BaTiO_3$ plasmonic photocatalysts, Journal of Alloys and Compounds, 801 (2019) 483-488.

[5] X. Zhou, Q. Sun, D. Zhai, G. Xue, H. Luo, D. Zhang, Excellent catalytic performance of molten-salt-synthesized $Bi_{0.5}Na_{0.5}TiO_3$ nanorods by the piezo-phototronic coupling effect, Nano Energy, 84 (2021).

[6] H. Sun, Z. Xu, X. Xie, J. Niu, M. Wang, X. Zhang, X. Chen, J. Han, Enhanced photocatalytic activity of ferroelectric-based $Ag_2O/Bi4Ti_3O_{12}$ hybrids by piezoelectric effect, Journal of Alloys and Compounds, 882 (2021) 160609.

[7] H. Xiao, W. Dong, Q. Zhao, F. Wang, Y. Guo, Visible/near-infrared light absorbed nano-ferroelectric for efficient photo-piezocatalytic water splitting and pollutants degradation, J Hazard Mater, 416 (2021) 125808.

[8] X. Jiang, H. Wang, X. Wang, G. Yuan, Synergetic effect of piezoelectricity and Ag

deposition on photocatalytic performance of barium titanate perovskite, Solar Energy, 224 (2021) 455-461.

[9] Y. Zhang, G. Shen, C. Sheng, F. Zhang, W. Fan, The effect of piezo-photocatalysis on enhancing the charge carrier separation in $BaTiO_3/KNbO_3$ heterostructure photocatalyst, Applied Surface Science, 562 (2021) 150164.

[10] X. Liao, T.-T. Li, H.-T. Ren, Z. Mao, X. Zhang, J.-H. Lin, C.-W. Lou, Enhanced photocatalytic performance through the ferroelectric synergistic effect of p-n heterojunction $BiFeO_3/TiO_2$ under visible-light irradiation, Ceramics International, 47 (2021) 10786-10795.

[11] L. Shi, C. Lu, L. Chen, Q. Zhang, Y. Li, T. Zhang, X. Hao, Piezocatalytic performance of $Na_{0.5}Bi_{0.5}TiO_3$ nanoparticles for degradation of organic pollutants, Journal of Alloys and Compounds, 895 (2022) 162591.

[12] J. Zou, H. Cai, D. Wang, J. Xiao, Z. Zhou, B. Yuan, Spectrophotometric determination of trace hydrogen peroxide via the oxidative coloration of DPD using a Fenton system, Chemosphere, 224 (2019) 646-652.

[13] H. Cai, X. Liu, J. Zou, J. Xiao, B. Yuan, F. Li, Q. Cheng, Multi-wavelength spectrophotometric determination of hydrogen peroxide in water with peroxidase-catalyzed oxidation of ABTS, Chemosphere, 193 (2018) 833-839.